






On the Performance Analysis of V2N Mixed RF and Hybrid FSO/RF Communication System

VSV Sandeep , Devendra S. Gurjar , Senior Member, IEEE, Suneel Yadav , Senior Member, IEEE, Prabina Pattanayak , Senior Member, IEEE, and Yuming Jiang , Senior Member, IEEE

Abstract—Vehicular communications allow vehicles to connect with other vehicles and network infrastructures in order to facilitate the transfer of real-time information and dependable transportation. This paper proposes a system that connects vehicles to the network (base station) in two phases using transceivers-equipped roadside infrastructures, such as signboards, traffic lights, and street lights, as intermediary relay nodes. In the first phase, the information transfer occurs from vehicles to infrastructure using a radio-frequency (RF) link. The second phase includes establishing communication from the infrastructure to the base station using hybrid free-space optics (FSO)/RF link. In modeling the FSO link, we consider factors like atmospheric attenuation, pointing errors, and atmospheric turbulence-induced fading, which can affect FSO performance. For this set-up, we derive the accurate expressions for the outage probability, system throughput, average symbol error rate, and average end-to-end delay. Numerical results corroborate the dependency of the time allocation factor α for the vehicle-to-infrastructure link on the vehicle transmit power. Furthermore, the results elucidate the impact of the length of the transmitted packet and FSO link distance on average end-to-end delay performance. The increase in distance between infrastructure and base station can be compensated by reducing the length of packets to achieve desirable delay performance.

Index Terms—Free-space optics (FSO), vehicle-to-network (V2N) communication, performance analysis, hybrid FSO/RF transmissions.

I. INTRODUCTION

WITH an alarming upsurge of vehicles in day-to-day lives, the need for safe transportation and vehicular interaction for coordination seems inevitable [1]. Technology companies and manufacturers seek to improve road safety and

Manuscript received 12 October 2022; revised 15 November 2022; accepted 18 November 2022. Date of publication 23 November 2022; date of current version 30 November 2022. An earlier version of this work was presented at the IEEE 95th Vehicular Technology Conference (VTC2022-Spring), Helsinki, Finland, June 2022. A part of this work was carried out during the tenure of an ERCIM “Alain Bensoussan” Fellowship Program. (Corresponding author: Devendra S. Gurjar.)

VSV Sandeep and Prabina Pattanayak are with the Department of Electronics and Communication Engineering, National Institute of Technology Silchar, Cachar 788010, India (e-mail: vavilapalli_pg@ece.nits.ac.in; prabina.pattanayak@ieeee.org).

Devendra S. Gurjar and Yuming Jiang are with the Department of Information Security and Communication Technology, Norwegian University of Science and Technology (NTNU), NO-7491 Trondheim, Norway (e-mail: devendra.gurjar@ieeee.org; yuming.jiang@ntnu.no).

Suneel Yadav is with the Department of Electronics and Communications Engineering, Indian Institute of Information Technology Allahabad, Allahabad 211012, India (e-mail: suneel@iiita.ac.in).

Digital Object Identifier 10.1109/JPHOT.2022.3223972

resilience by exploiting vehicle-to-everything (V2X) connectivity, citing the possibility that advanced vehicular networking might cut over 80% of road accidents [2]. In fact, V2X communication can potentially ameliorate transportation systems in numerous ways, from collision avoidance to energy-efficient systems [3]. With onboard communication modules, automated vehicular networks have become a reality. The vehicles can be made to safely communicate with each other and interact with roadside infrastructures such as traffic lights, signboards, etc., using appropriate wireless communication protocols [4]. The United States Federal Communications Commission (FCC) adopted a report to establish licensing and service rules for the dedicated short-range communications (DSRC) utilizing 5.850–5.925 GHz of 5.9 GHz band in 2003 [5]. Further, in November 2020, the FCC reallocated the lower 45 MHz band, i.e., 5.850–5.895 GHz for the expansion of unlicensed mid-band spectrum operations, while continuing to dedicate the upper 30 MHz portion of the same band, i.e., 5.895–5.925 GHz for the intelligent transportation system operations [6]. The scope to create a large-scale network to meet the expanding needs of vehicular communications is still a challenging task due to the spectrum scarcity, reliability, dynamic resource allocation, low data rates, delay, and security concerns posed by increasing number of vehicles.

In order to address spectrum scarcity, significant efforts have been made to enable V2X communications relying on the mmWave frequencies [7], [8], [9], [10]. With mmWave access, vehicular communications can be realized with huge bandwidth and low latency, which may expedite the development of autonomous driving vehicles [11]. However, the mmWave channel faces several challenges, such as high mobility, blockages, high transmission loss, etc. To compensate for high transmission loss, mmWave transmitters can utilize directional transmissions, often referred to as a mmWave beam [12]. Mobility management is another prominent issue with direct transmission, especially for mmWave-based vehicular communication. As per Release 16 of the third generation partnership project (3GPP), vehicles face different types of mobility with mmWave transmission, e.g., beam level and cell level mobility [12]. Still, there are many open issues that need to be resolved before implementing mmWave-based transmission in practical vehicular communication scenarios.

On the other hand, the traditional methods of spectrum re-structuring and cell densification have proven inefficient in addressing the needs of an exponential rise in emerging

wireless technologies and applications seeking higher data rates, leaving us in search of a new technique as a possible solution. Optical wireless communications (OWC) can become a potential solution for dealing with such increased data rate requirements [13], [14]. Analogous to radio-frequency (RF) transmission, OWC allows information transmission in an unguided medium, such as free space, utilizing infrared, visible light, and ultraviolet bands. Based on the carrier, OWC can be categorized as free-space optics (FSO), visible light communications (VLC), and ultraviolet communications. To realize FSO transmission, it requires the presence of line-of-sight (LoS) link between transmitter and receiver and uses a near-infrared band for information transmission [15], [16]. Due to its operation in the near-infrared band, FSO offers inherent advantages in terms of increased bandwidth, thus resulting in higher achievable data rates. Owing to the narrow laser beam used in transmission, FSO delivers spatial confinement that allows greater frequency reuse, better security, and immunity to electromagnetic interference. Despite several advantages, physical phenomena, such as atmospheric turbulence-induced fading, pointing errors, and atmospheric attenuation, severely affect the performance of FSO-based systems. As such, atmospheric turbulence-induced fading appears as a sequence of variations in the refractive index caused by temperature and atmospheric pressure changes. The misalignment of transmitter and receiver due to the swaying of buildings causes pointing or geometric and misalignment errors. Further, atmospheric attenuation is present due to particles' absorption and scattering in the atmosphere.

Due to the inherent benefits of FSO, various recent works have considered FSO communication as one of the links in establishing multi-hop end-to-end communication. In [17], the authors have investigated a dual-hop mixed RF and FSO network considering amplify-and-forward (AF) relaying, where Nakagami- m and double generalized Gamma distributions are assumed for RF and FSO links, respectively. They have examined the system performance in terms of ergodic capacity, outage probability, and bit error rate (BER). Likewise, the authors in [18] have conducted the performance analysis for a decode-and-forward (DF) relaying based dual-hop mixed RF and FSO system assuming Malaga distribution to model FSO link and Nakagami- m distribution to model RF link. In [19], the authors have considered a hybrid RF/FSO system in establishing a 5G radio access network where the RF link is modeled using $\kappa - \mu$ distribution and the FSO link is modeled via exponentiated Weibull distribution. For the considered network, the performance has been evaluated in terms of outage probability, BER, and ergodic capacity.

To increase the reliability of FSO communications, recent works in [20], [21], [22] have considered an RF link as a backup link to the primary FSO link. Specifically in [20], the authors have evaluated the performance of a hybrid FSO/RF network in terms of outage probability and BER by assuming Nakagami- m distribution for the RF link and Gamma-Gamma distribution for the FSO link. The authors in [21] have investigated a hybrid FSO/RF network by considering generalized distributions in modeling FSO and RF links, i.e., Malaga and $\alpha - \eta - \kappa - \mu$ distributions for FSO and RF links, respectively. In [20] and [21], performance analysis has been carried out by considering a

single-user scenario. In [22], the authors have analyzed the system's performance in terms of outage probability and BER for a relay-assisted multi-user hybrid FSO/RF communication system. However, all the aforementioned works were carried out under the assumption where all the nodes were stationary.

The works in [23], [24], [25], [26] have characterized the mobility aspect of vehicles with the help of a first-order autoregressive process. In [23] and [26], the authors have considered only the RF links for enabling communication. Whereas in [24], the authors have introduced a mixed MIMO RF and FSO system and investigated the performance in terms of outage probability, BER, ergodic capacity, and asymptotic analysis. Herein, the RF link has been modeled using the Rayleigh distribution and the FSO link using the Gamma-gamma distribution. By considering mixed MIMO orthogonal space-time block code, and FSO co-operative system using DF relaying, the authors in [25] have obtained exact and asymptotic expressions of outage probability and bit error probability.

A. Background and Motivation

The existing radio access technologies (RATs) for vehicular communication are DSRC and cellular-V2X (C-V2X) [27], [28], [29], [30], [31]. Both DSRC and C-V2X are undergoing comprehensive improvement to support advanced vehicular applications. The upgraded versions of these RATs are IEEE 802.11bd for DSRC and NR V2X for C-V2X, which can supplement autonomous driving operations. Both are different in the design methodology, but they have certainly similar design objectives, e.g., better reliability of offered services, low end-to-end latency, and the ability to support applications that require high throughput. In a dense urban environment, the number of vehicles occupying road space can be innumerable. As a result, DSRC may experience substantial RF interference in such scenarios, leading to greater re-transmissions and higher transmission delay. Thus, to allow communication between vehicles located farther distances apart, DSRC seems to be an unreliable solution. On the other hand, cellular-V2X operates on the licensed spectrum for enabling vehicular communications, which was introduced by the 3GPP for the first time in Release 14 [28]. Further, the 5G NR V2X communication has been standardized in Release 16, where the main focus is on improving reliability, capacity, and flexibility while minimizing latency. The use cases for this release are not only limited to road safety but also include advanced attributes such as platooning, extended sensors, autonomous driving [29]. In establishing communication for vehicle-to-network (V2N), the allocation of resources to vehicles is done at the network, i.e., eNodeB or ngnodeB, unlike in the case of vehicle-to-vehicle, vehicle-to-infrastructure (V2I), and vehicle-to-pedestrian communications, where vehicles automatically do the resource allocation by sensing the environment. Thus, more vehicles trying to communicate in dense urban environments may lead to congestion in spectrum assignment. Consequently, radio resource allocation can significantly affect the performance of cellular V2N communication. This is not the case with FSO-based communication since it provides enormous bandwidth. In 5G NR V2X, vehicles trying

to access the network may compromise information security, which demands the usage of advanced coding and encryption for secure information transfer. Also, it increases extra packet headers along with information leading to more significant latency. In contrast, FSO transmission provides greater spatial confinement and minor beam deviation, thus can achieve better security.

Although FSO-based networks can deliver huge data rates and ultra-low latency, their performance can be significantly limited due to atmospheric turbulence and the necessity of LoS if used as standalone systems. Thus, considering an RF link as a backup for the FSO link can be a feasible solution for reliable V2N communication. Motivated by this, we introduce a dual-hop hybrid FSO/RF system. Herein, a standalone RF link is utilized during the first transmission phase to facilitate information transmission between vehicles and roadside infrastructure. In the next phase, a hybrid FSO/RF link operates to enable communication between the infrastructure and the base station. The FSO link is aided by the RF link to minimize the impact of atmospheric turbulence, thus making the system more reliable. The infrastructure node performs a DF operation to relay the signal received from a vehicle to the base station. It is assumed that the moving vehicles cause the channels time-varying in nature, which can be modeled as a first-order Markovian process. Further, FSO link's irradiance fluctuates as a sequence of atmospheric attenuation, atmospheric turbulence-induced fading, and pointing errors. For this setup, we derive accurate expressions for the outage probability, system throughput, average symbol error rate (SER), and average end-to-end delay.

B. Contributions

The primary objective of this work is to implement a robust and reliable large-scale network to enable communication for vehicles located at a farther distance apart. The major contributions of our paper can be summarized as follows:

- We consider mixed RF and hybrid FSO/RF transmissions for V2N communication by taking into account all the factors that can affect FSO performance, i.e., atmospheric turbulence-induced fading, misalignment errors, and atmospheric attenuation.
- By considering the mobility of the vehicle in modeling the V2I link, the time selective fading nature of the V2I link is characterized using a first-order auto-regression process. The effect of the relative speed of the vehicle and the vehicle transmit power on the considered performance metrics are assessed.
- We proficiently derive the closed-form expressions for outage probability, average SER, and average end-to-end delay of the system by considering all the intricacies involved in obtaining the expressions for the multi-hop network.
- We disclose the impacts of various system design and channel parameters on the considered performance metrics of the system. Specifically, the effect of pointing errors and atmospheric turbulence-induced fading on the average end-to-end delay performance of the system is studied.

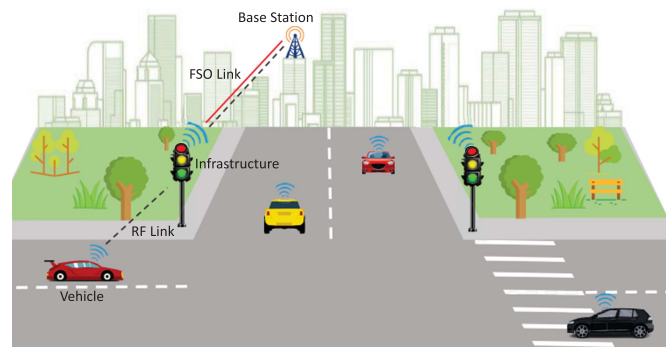


Fig. 1. A V2N communication system with hybrid RF/FSO transmissions.

Also, the impact of FSO link distance and length of the transmitted packet on delay performance is investigated.

C. Organization

The rest of the paper is organized as follows. In Section II, we present the system model, and derive the instantaneous SNR expression for V2I RF link and individual instantaneous SNR expressions for FSO and RF links of hybrid FSO/RF channel. In Section III, the closed-form expressions for the outage probability, system throughput, average SER, and average end-to-end delay are derived. In Section IV, the numerical and simulation results with a detailed discussion on the influence of various system/channel parameters on the system's performance are described, followed by the conclusions in Section V.

Notations: Throughout of this paper, we use \triangleq to denote the equality by definition, and $\mathbb{E}[X]$ denotes the expectation of a random variable X . $f_X(\cdot)$ and $F_X(\cdot)$ denote the probability density function (PDF) and cumulative distribution function (CDF), respectively. $\Gamma(a)$ and $\Upsilon(a, x)$ denote the incomplete Gamma function and lower incomplete Gamma function [32, eq. (8.350)], and $\text{erf}(\cdot)$ and $\text{erfc}(\cdot)$ are the error function and complementary error function, respectively [32, eq. (8.250)]. $\mathcal{K}_\nu(\cdot)$ denotes the ν -th order modified Bessel function of second kind [32, eq. (8.432)] and $\mathcal{G}_{p,q}^{m,n}(x|_{b_1, \dots, b_q}^{a_1, \dots, a_p})$ represents the Meijer- \mathcal{G} function [32, eq. (9.301)].

II. SYSTEM MODEL

We consider a vehicular communication scenario as depicted in Fig. 1 where a vehicle communicates to the base station using the relay cooperation from transceiver-mounted traffic lights as in [33]. One round of information transmission from a vehicle to the base station is completed in two phases. First, the vehicle communicates with the infrastructure using an RF link. Then, a hybrid FSO/RF link is used in the second phase for establishing information transmission from the infrastructure and the base station. In the second phase, only one link will be involved in communication at a time to increase the system's energy efficiency. In particular, the FSO link is employed as a main link having RF link as backup. The RF link becomes active only when the instantaneous signal-to-noise ratio (SNR) corresponding to the FSO link drops below a specified target SNR. A feedback bit

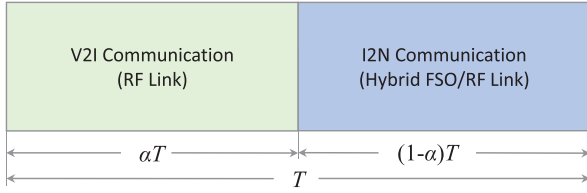


Fig. 2. Transmission block structure.

is used for sending information about the switching from FSO to RF links, considering perfect channel state information (CSI). We consider that the RF channels experience the Nakagami- m fading. In characterizing FSO link, we use Gamma-Gamma and Rayleigh distributions to model atmospheric turbulence-induced fading and pointing errors, respectively [34], [35]. Further, one transmission block of duration T is split into two slots of αT and $(1 - \alpha)T$ duration, as illustrated in Fig. 2, where $\alpha \in (0, 1)$ denotes time factor.

A. SNR for Vehicle-to-Infrastructure RF Link

Using an RF link, the vehicle communicates to the infrastructure with unit energy signal x_V during the first transmission phase. The received signal can be expressed as

$$y_I = \sqrt{P_V} h_{V,I} x_V + n_I, \quad (1)$$

where P_V represents vehicle's transmit power, $h_{V,I}$ denotes the channel gain for vehicle to infrastructure link, and $n_I \in \mathcal{CN}(0, \sigma_I^2)$ is considered to be additive white Gaussian noise (AWGN). For characterizing the mobility¹, $h_{V,I}$ can be modeled as first-order auto-regression process [26], [37]

$$h_{V,I} = \rho \bar{h}_{V,I} + \sqrt{1 - \rho^2} h_{e_I}, \quad (2)$$

where ρ is correlation coefficient between $h_{V,I}$ and $\bar{h}_{V,I}$. It can be obtained using Jake's model as $\rho = \mathcal{J}_0\left(\frac{2\pi f_c v_s T_d}{c}\right)$, where $\mathcal{J}_0(\cdot)$ represents zeroth-order Bessel function of first kind [32, eq. (8.402)], f_c is carrier frequency, and v_s is the relative velocity. T_d denotes transmitted symbol duration, and c represents the velocity of light in free space. Further, $h_{e_I} \in \mathcal{CN}(0, \Omega_e)$ is the error component of channel gain.

Now, on incorporating (2) in (1), we can get

$$y_I = \sqrt{P_V \rho} \bar{h}_{V,I} x_V + \sqrt{P_V (1 - \rho^2)} h_{e_I} x_V + n_I. \quad (3)$$

Following (3), the instantaneous SNR at the infrastructure can be given as

$$\gamma_{V,I} = \frac{P_V \rho^2 |\bar{h}_{V,I}|^2}{P_V (1 - \rho^2) \Omega_e + \sigma_I^2}. \quad (4)$$

Further, the instantaneous capacity pertaining to the V2I link can be expressed as $C_{V,I} = \alpha \log_2(1 + \gamma_{V,I})$.

¹It is important to note that in this work, we consider a first-order auto-regression process to model the vehicle's mobility with perfect channel estimates, where the assumption of perfect CSI is based on the fact that the tracking loops at the fixed infrastructure and the base station can correctly estimate the channel coefficients related to the first transmitted symbol of each block [36]. The joint consideration of node's mobility and imperfect channel estimates under this system setup is left for the future study.

B. SNRs for Infrastructure-to-Network FSO/RF Link

1) *SNR for FSO Link*: By assuming the direct detection technique, the received FSO signal at the base station can be given as

$$y_N^{\text{FSO}} = P_{I_F} \eta \mathcal{I}_F x_{I_F} + n_{N_F}, \quad (5)$$

where P_{I_F} denotes infrastructure's transmit power for FSO communication, η represents a factor for the optical-to-electrical power conversion, x_{I_F} is the unit energy symbol, $n_{N_F} \in \mathcal{CN}(0, \sigma_{N_F}^2)$ represents the AWGN at the base station, and \mathcal{I}_F denotes the irradiance/intensity of the FSO link. Also, \mathcal{I}_F is mainly affected by the atmospheric turbulence-induced fading (\mathcal{I}_a), pointing errors (\mathcal{I}_p), and atmospheric attenuation (\mathcal{I}_l), and hence can be mathematically represented as $\mathcal{I}_F = \mathcal{I}_a \mathcal{I}_p \mathcal{I}_l$.

On utilizing (5), the instantaneous SNR at the base station for FSO transmission can be expressed as

$$\gamma_{I,N}^{\text{FSO}} = \frac{P_{I_F}^2 \eta^2 \mathcal{I}_F^2}{\sigma_{N_F}^2} = \frac{\mathcal{I}_F^2}{(\mathbb{E}\{\mathcal{I}_F\})^2} \bar{\gamma}_{I,N}^{\text{FSO}}. \quad (6)$$

where $\mathcal{I}_F = \mathcal{I}_a \mathcal{I}_p \mathcal{I}_l$ and $\bar{\gamma}_{I,N}^{\text{FSO}} = \frac{P_{I_F}^2 \eta^2 (\mathbb{E}\{\mathcal{I}_F\})^2}{\sigma_{N_F}^2}$ denotes the average electrical SNR of the FSO link at the base station.

Moreover, the instantaneous capacity corresponding to infrastructure-to-network (I2N) link for FSO communication can be given as $C_{I,N}^{\text{FSO}} = (1 - \alpha) \log_2(1 + \gamma_{I,N}^{\text{FSO}})$.

2) *SNR for RF Link*: The received RF signal at the base station can be expressed as

$$y_N = \sqrt{P_I} h_{I,N} x_V + n_N, \quad (7)$$

where P_I denotes transmit power at the infrastructure node for RF transmission, $h_{I,N}$ represents channel gain of the RF link, x_V denotes unit energy symbol, and $n_N \in \mathcal{CN}(0, \sigma_N^2)$ is the AWGN at the base station. Using (7), the instantaneous SNR at the base station for the RF link can be obtained as

$$\gamma_{I,N}^{\text{RF}} = \frac{P_I |h_{I,N}|^2}{\sigma_N^2}. \quad (8)$$

The instantaneous capacity of I2N link for RF communication can be expressed as $C_{I,N}^{\text{RF}} = (1 - \alpha) \log_2(1 + \gamma_{I,N}^{\text{RF}})$.

III. PERFORMANCE ANALYSIS

In this section, we first obtain the CDF and PDF of $|\bar{h}_{V,I}|^2$, $|h_{I,N}|^2$, \mathcal{I}_a , and \mathcal{I}_p . We also present the modeling of atmospheric attenuation \mathcal{I}_l . Then, we exploit them to evaluate the expressions for outage probability, system throughput, average SER, and average end-to-end delay for the considered system.

A. The PDFs and CDFs of $|\bar{h}_{V,I}|^2$, $|h_{I,N}|^2$, \mathcal{I}_a , and \mathcal{I}_p , and Modeling of \mathcal{I}_l

1) *The PDFs and CDFs of $|\bar{h}_{V,I}|^2$ and $|h_{I,N}|^2$* : It is worthwhile to note that the channel coefficients $\bar{h}_{V,I}$ and $h_{I,N}$ corresponding to RF communication follow Nakagami- m distribution. Therefore, the channel gains $|\bar{h}_{V,I}|^2$ and $|h_{I,N}|^2$ follow the

Gamma distribution, whose CDF and PDF can be expressed as

$$f_{Y \in \{|\bar{h}_{V,1}|^2, |h_{L,N}|^2\}}(y) = \frac{\left(\frac{m_\iota}{\Omega_\iota}\right)^{m_\iota}}{\Gamma[m_\iota]} y^{m_\iota-1} e^{-\frac{m_\iota}{\Omega_\iota} y}, y \geq 0, \quad (9)$$

$$F_{Y \in \{|\bar{h}_{V,1}|^2, |h_{L,N}|^2\}}(y) = \frac{1}{\Gamma[m_\iota]} \Upsilon\left(m_\iota, \frac{m_\iota}{\Omega_\iota} y\right), y \geq 0, \quad (10)$$

where $\iota = \text{I}$ when $Y = |\bar{h}_{V,1}|^2$ and $\iota = \text{N}$ when $Y = |h_{L,N}|^2$.

2) *The PDF and CDF of Atmospheric Turbulence Induced Fading (\mathcal{I}_a):* We consider \mathcal{I}_a to follow the Gamma-Gamma distribution. Thus, we obtain \mathcal{I}_a by finding the product of two independent Gamma distributions, i.e., $\mathcal{I}_a = X_1 X_2$, where X_1 denotes the effect of large-scale turbulence and X_2 shows the impact of the small scale turbulence. The PDFs of X_1 and X_2 can be expressed as

$$f_{X_1}(v) = \frac{\varpi^\varpi}{\Gamma[\varpi]} v^{\varpi-1} e^{-\varpi v}, v \geq 0, \varpi > 0, \quad (11)$$

$$f_{X_2}(w) = \frac{\beta^\beta}{\Gamma[\beta]} w^{\beta-1} e^{-\beta w}, w \geq 0, \beta > 0. \quad (12)$$

Further, the PDF and CDF of \mathcal{I}_a is obtained as per the following proposition.

Proposition 1: The PDF and CDF expressions of \mathcal{I}_a under Gamma-Gamma distribution are obtained, respectively, as

$$f_{\mathcal{I}_a}(x) = \frac{2(\varpi\beta)^{\frac{\varpi+\beta}{2}}}{\Gamma(\varpi)\Gamma(\beta)} x^{\frac{\varpi+\beta}{2}-1} \mathcal{K}_{\varpi-\beta}(2\sqrt{\varpi\beta x}), \quad (13)$$

$$F_{\mathcal{I}_a}(x) = \frac{(\varpi\beta)^{\frac{\varpi+\beta}{2}}}{\Gamma(\varpi)\Gamma(\beta)} x^{\frac{\varpi+\beta}{2}} \mathcal{G}_{1,3}^{2,1}\left(\varpi\beta x \middle| \frac{2-\varpi-\beta}{2}, -\frac{\varpi-\beta}{2}, -\frac{\varpi-\beta}{2}\right). \quad (14)$$

Proof: See Appendix A. ■

3) *The PDF and CDF of Pointing Errors (\mathcal{I}_p):* Assuming the transmitted beam follows Gaussian distribution with the detector's radius of a , pointing error r . Accordingly, power collected at the detector can be expressed as [38]

$$\mathcal{I}_p(r, z) \approx A_0 e^{-\frac{2|r|^2}{w_{zeq}^2}}, \quad (15)$$

where A_0 denotes peak irradiance considering $r = 0$, w_{zeq} represents equivalent beam width which can be expressed as $w_{zeq}^2 = \frac{w_0^2 \text{erf}(\nu)}{2\nu e^{-\nu^2}}$ with $\nu = \frac{\sqrt{\pi}a}{\sqrt{2}w_z}$ and $A_0 = \text{erf}(\nu)^2$. Further, $w_z \approx w_0 \sqrt{1 + \epsilon\left(\frac{\lambda z}{\pi w_0^2}\right)^2}$, where z denotes the FSO link distance. For $z = 0$, $w_z \approx w_0$, thus w_0 is the beam radius of beam waist. Also, $\epsilon = 1 + \frac{2w_0^2}{\rho_0(z)^2}$, where $\rho_0(z)$ is the coherence radius given as $\rho_0(z) = (0.55C_n^2 k^2 z)^{-3/5}$ with C_n^2 as the refractive index parameter and $k = \frac{2\pi}{\lambda}$ as the wave number.

Further, one can get the pointing error r by performing the sum of horizontal displacement and elevation. On assuming that horizontal displacement and elevation follow independent Gaussian distributions, $|r|$ will follow the Rayleigh distribution, and therefore, the PDF of $|r|$ can be obtained as

$$f_{|r|}(r) = \frac{r}{\sigma_s^2} e^{-\frac{r^2}{2\sigma_s^2}}, r \geq 0, \quad (16)$$

where σ_s^2 represents displacement variance of pointing error.

Moreover, the PDF and CDF of pointing error, \mathcal{I}_p , can be evaluated according to the below proposition.

Proposition 2: The PDF and CDF of \mathcal{I}_p under Rayleigh fading channels can be given, respectively, as

$$f_{\mathcal{I}_p}(y) = \frac{g^2}{(A_0)^{g^2}} y^{g^2-1}, \quad (17)$$

$$F_{\mathcal{I}_p}(y) = \left(\frac{y}{A_0}\right)^{g^2}, \quad (18)$$

for $0 \leq y \leq A_0$.

Proof: Combining (15) and (16) with variable transformation, the PDF of \mathcal{I}_p can be expressed as

$$\begin{aligned} f_{\mathcal{I}_p}(y) &= f_{|r|} \left(\sqrt{\frac{w_{zeq}^2}{2} \ln\left(\frac{A_0}{y}\right)} \right) \frac{\partial}{\partial y} \left(\sqrt{\frac{w_{zeq}^2}{2} \ln\left(\frac{A_0}{y}\right)} \right), \\ &= \frac{w_{zeq}^2}{4y\sigma_s^2} e^{\left(\ln\left(\frac{y}{A_0}\right)\right) \frac{w_{zeq}^2}{4\sigma_s^2}} = \frac{g^2}{(A_0)^{g^2}} y^{g^2-1}, \end{aligned} \quad (19)$$

for $0 \leq y \leq A_0$, where $g \triangleq \frac{w_{zeq}}{2\sigma_s}$.

Further, by applying the relation $F_{\mathcal{I}_p}(y) = \int_0^y f_{\mathcal{I}_p}(y) dy$ and utilizing (19), we can obtain the CDF of \mathcal{I}_p as presented in (18). This completes the proof. ■

4) *Modeling of Atmospheric Attenuation (\mathcal{I}_l):* Utilizing Lambert's law [39], the power at a distance L can be related to emitted power of the source as

$$\mathcal{I}_l = \frac{P(\lambda, L)}{P(\lambda, 0)} = e^{-\Xi(\lambda)L}, \quad (20)$$

where λ is the wavelength, $P(\lambda, 0)$ denotes the emitted power, $P(\lambda, L)$ represents the signal power at a distance L , and $\Xi(\lambda)$ represents the extinction coefficient which relies on the wavelength and can be obtained as the sum of scattering and absorption coefficients.

B. Outage Probability Analysis

For the considered system, an outage event happens if the RF signal is not decoded successfully in the first phase at the relaying infrastructure or instantaneous SNRs corresponding to both FSO and RF communications in the second phase fall shorter to meet a specific threshold SNRs. With this, the outage probability can be defined as

$$\mathcal{P}_{\text{out}} = 1 - \mathcal{P}_{\text{dec}}(1 - \mathcal{P}_{\text{FSO}}\mathcal{P}_{\text{RF}}), \quad (21)$$

where \mathcal{P}_{dec} depicts successful decoding probability in the first phase at the relaying infrastructure, and \mathcal{P}_{FSO} and \mathcal{P}_{RF} represent the probabilities of link failure at the base station for FSO and RF transmissions, respectively, in the second phase.

1) *Evaluation of \mathcal{P}_{dec} :* The decoding probability at infrastructure node in the first transmission phase can be given as

$$\begin{aligned} \mathcal{P}_{\text{dec}} &= 1 - \Pr[\mathcal{C}_{V,1} < r_{\text{th}}] \\ &= 1 - \Pr[\alpha \log_2(1 + \gamma_{V,1}) < r_{\text{th}}] \end{aligned}$$

$$= 1 - \Pr \left[|\bar{h}_{V,I}|^2 < \frac{\varphi_{\text{th}}(P_V(1-\rho^2)\Omega_e + \sigma_I^2)}{P_V\rho^2} \right], \quad (22)$$

where $\varphi_{\text{th}} = 2^{\frac{r_{\text{th}}}{\alpha}} - 1$ denotes the target SNR of RF link at the relaying infrastructure, and r_{th} represents the preset target data rate (in bps/Hz).

Now, utilizing (10) into (22), \mathcal{P}_{dec} , can be obtained as

$$\mathcal{P}_{\text{dec}} = 1 - \frac{1}{\Gamma[m_I]} \Upsilon \left[m_I, \frac{m_I\varphi_{\text{th}}(P_V(1-\rho^2)\Omega_e + \sigma_I^2)}{\Omega_I P_V \rho^2} \right]. \quad (23)$$

2) *Evaluation of \mathcal{P}_{FSO}* : The outage event occurs for the FSO link when the corresponding instantaneous SNR falls below the target SNR, and thus the FSO link's failure probability can be mathematically formulated as

$$\begin{aligned} \mathcal{P}_{\text{FSO}} &= \Pr \left[\mathcal{C}_{I,N}^{\text{FSO}} = (1-\alpha) \log_2(1 + \gamma_{I,N}^{\text{FSO}}) < r_{\text{th}} \right], \\ &= \Pr \left[\gamma_{I,N}^{\text{FSO}} < \varphi_{\text{th}}^{\text{FSO}} \right], \end{aligned} \quad (24)$$

where $\varphi_{\text{th}}^{\text{FSO}} = 2^{\frac{r_{\text{th}}}{1-\alpha}} - 1$ is the target SNR of FSO transmission at the base station. Further, \mathcal{P}_{FSO} can be evaluated as per Theorem 1.

Theorem 1: The probability of link failure of FSO link, \mathcal{P}_{FSO} , under Gamma-Gamma distribution can be expressed as

$$\mathcal{P}_{\text{FSO}} = \frac{g^2}{\Gamma[\varpi]\Gamma[\beta]} \mathcal{G}_{2,4}^{3,1} \left[\varpi\beta\mu \sqrt{\frac{\varphi_{\text{th}}^{\text{FSO}}}{\bar{\gamma}_{I,N}^{\text{FSO}}}} \middle| \begin{matrix} 1, g^2+1 \\ g^2, \varpi, \beta, 0 \end{matrix} \right]. \quad (25)$$

where $\mu = \frac{g^2}{g^2+1}$ and $\bar{\gamma}_{I,N}^{\text{FSO}} = \frac{P_F^2 \eta^2 (A_0 \mu I_i)^2}{\sigma_{\text{NF}}^2}$.

Proof: See Appendix B for the detailed derivation. ■

3) *Evaluation of \mathcal{P}_{RF}* : The probability of failure of the RF link at the base station can be formulated as

$$\begin{aligned} \mathcal{P}_{\text{RF}} &= \Pr \left[\frac{P_I |h_{I,N}|^2}{\sigma_N^2} < \varphi_{\text{th}}^{\text{RF}} \right], \\ &= \Pr \left[|h_{I,N}|^2 < \frac{\sigma_N^2 \varphi_{\text{th}}^{\text{RF}}}{P_I} \right], \end{aligned} \quad (26)$$

where $\varphi_{\text{th}}^{\text{RF}} = 2^{\frac{r_{\text{th}}}{1-\alpha}} - 1$ is the threshold SNR of RF link at the base station. Now, exploiting the CDF of $|h_{I,N}|^2$ from (10) into (26), we can obtain \mathcal{P}_{RF} as

$$\mathcal{P}_{\text{RF}} = \frac{1}{\Gamma[m_N]} \Upsilon \left[m_N, \frac{m_N \sigma_N^2 \varphi_{\text{th}}^{\text{RF}}}{\Omega_N P_I} \right]. \quad (27)$$

On utilizing (23), (25), and (27) into (21), one can obtain the desired expression for outage probability of the considered system.

C. System Throughput

Considering a delay-limited scenario, the system throughput can be defined using outage probability expression and the threshold data rate, as [40]

$$S_T = (1 - \mathcal{P}_{\text{out}}) r_{\text{th}}, \quad (28)$$

where r_{th} is threshold data rate in bps/Hz.

D. Average Symbol Error Rate (SER)

For a dual-hop DF relaying scheme by considering independent fading channels for individual hops, the average SER can be expressed as [18]

$$\mathcal{P}_{\text{SER}} = \mathcal{P}_{\text{SER,I}} + \mathcal{P}_{\text{SER,N}} - 2 \mathcal{P}_{\text{SER,I}} \mathcal{P}_{\text{SER,N}}, \quad (29)$$

where $\mathcal{P}_{\text{SER,I}}$ is the average SER of V2I link and $\mathcal{P}_{\text{SER,N}}$ is the average SER of I2N link. To proceed further, we first need to obtain the average SER of V2I link $\mathcal{P}_{\text{SER,I}}$, and the average SER of I2N link, $\mathcal{P}_{\text{SER,N}}$.

1) *Average SER of V2I RF Link*: The average SER of V2I link during non-outage event can be given as [38]

$$\mathcal{P}_{\text{SER,I}} = \frac{\mathcal{A}}{2} \int_{\varphi_{\text{th}}}^{\infty} \text{erfc}(\mathcal{B}\sqrt{x}) f_{\gamma_{V,I}}(x) dx, \quad (30)$$

with \mathcal{A} and \mathcal{B} are the values taken depending on the M -ary PSK modulation scheme used for communication. For $M = 2$, the parameters $\mathcal{A} = 1$ and $\mathcal{B} = \sin(\frac{\pi}{2})$, whereas for the case when $M > 2$, we have $\mathcal{A} = 2$ and $\mathcal{B} = \sin(\frac{\pi}{M})$. Furthermore, by using the integration by parts, we can express $\mathcal{P}_{\text{SER,I}}$ in (30) as

$$\begin{aligned} \mathcal{P}_{\text{SER,I}} &= \frac{\mathcal{A}}{2} \text{erfc}(\mathcal{B}\sqrt{x}) \int_{\varphi_{\text{th}}}^{\infty} f_{\gamma_{V,I}}(x) dx \\ &\quad - \frac{\mathcal{A}}{2} \int_{\varphi_{\text{th}}}^{\infty} \left[\frac{\partial}{\partial x} \text{erfc}(\mathcal{B}\sqrt{x}) \right] \left(\int_{\varphi_{\text{th}}}^{\infty} f_{\gamma_{V,I}}(x) dx \right) dx. \end{aligned} \quad (31)$$

On substituting the PDF of $\gamma_{V,I}$ (which can be obtained on taking the derivative of (23) with the aid of $\frac{\partial}{\partial z} \Upsilon(\alpha, z) = z^{\alpha-1} e^{-z}$ [32, eq. (8.356.4)]) into (31), and carrying out the required integration by following the same approach as used in [41] and with the assistance of $\frac{\partial}{\partial x} \text{erfc}(\mathcal{B}\sqrt{x}) = -\frac{\mathcal{B}}{\sqrt{\pi}} x^{-\frac{1}{2}} e^{-\mathcal{B}^2 x}$ and [32, eqs. (2.33.10), (2.33.5)] to obtain

$$\begin{aligned} \mathcal{P}_{\text{SER,I}} &= \frac{\mathcal{A}}{2} \frac{1}{\Gamma[m_I]} \text{erfc}(\mathcal{B}\sqrt{\varphi_{\text{th}}}) \Gamma \left(m_I, \frac{m_I}{\Omega_I \xi} \varphi_{\text{th}} \right) \\ &\quad - \frac{\mathcal{A}\mathcal{B}}{2\sqrt{\pi}} \sum_{n=0}^{m_I-1} \frac{1}{n!} \frac{\Gamma \left(n + \frac{1}{2}, (\mathcal{B}^2 + \frac{m_I}{\Omega_I \xi}) \varphi_{\text{th}} \right)}{(\mathcal{B}^2 + \frac{m_I}{\Omega_I \xi})^{n+\frac{1}{2}}} \left(\frac{m_I}{\Omega_I \xi} \right)^n. \end{aligned} \quad (32)$$

where $\xi = \frac{P_V \rho^2}{P_V(1-\rho^2)\Omega_e + \sigma_I^2}$.

2) *Average SER of I2N Hybrid FSO/RF Link*: For the I2N communication link, the average SER depends on two events, viz., when the FSO link is active, and when the FSO link is in outage (i.e., the backup RF link is active). Thus, the average SER for the I2N hybrid FSO/RF link can be expressed as [21]

$$\mathcal{P}_{\text{SER,N}} = \mathcal{P}_{\text{SER,N}}^{\text{FSO}} + \mathcal{P}_{\text{FSO}} \mathcal{P}_{\text{SER,N}}^{\text{RF}}, \quad (33)$$

where $\mathcal{P}_{\text{SER,N}}^{\text{FSO}}$ and $\mathcal{P}_{\text{SER,N}}^{\text{RF}}$ are the average SERs of FSO and RF links for I2N communication link, respectively. To evaluate $\mathcal{P}_{\text{SER,N}}$, we first obtain the expressions for $\mathcal{P}_{\text{SER,N}}^{\text{FSO}}$ and $\mathcal{P}_{\text{SER,N}}^{\text{RF}}$, in what follows.

i) *Evaluation of $\mathcal{P}_{SER,N}^{FSO}$* : The average SER of I2N FSO link can be formulated as

$$\mathcal{P}_{SER,N}^{FSO} = \int_{\varphi_{th}^{FSO}}^{\infty} p(e/x) f_{\gamma_{I,N}^{FSO}}(x) dx. \quad (34)$$

where

$$p(e/x) = \frac{\mathcal{A}}{2} \operatorname{erfc}(\mathcal{B}\sqrt{x}). \quad (35)$$

To solve (34), we require the expression of $f_{\gamma_{I,N}^{FSO}}(x)$, which can be obtained by differentiating the CDF presented in (52) with respect to x as

$$\begin{aligned} f_{\gamma_{I,N}^{FSO}}(x) &= \frac{\partial}{\partial x} \left[F_{\mathcal{I}_F} \left(\mu A_0 \mathcal{I}_l \sqrt{\frac{x}{\gamma_{I,N}^{FSO}}} \right) \right] \\ &= \frac{\mu A_0 \mathcal{I}_l}{2\sqrt{\gamma_{I,N}^{FSO} x}} f_{\mathcal{I}_F} \left(\mu A_0 \mathcal{I}_l \sqrt{\frac{x}{\gamma_{I,N}^{FSO}}} \right) \\ &\stackrel{(a)}{=} \frac{g^2}{2\Gamma[\varpi]\Gamma[\beta]} \frac{1}{x} \mathcal{G}_{1,3}^{3,0} \left[\varpi \beta \mu \sqrt{\frac{x}{\gamma_{I,N}^{FSO}}} \middle| \begin{matrix} g^2+1 \\ g^2, \varpi, \beta \end{matrix} \right], \end{aligned} \quad (36)$$

where (a) is obtained by substituting the PDF expression given in (56) and with the use of [32, eq. (9.31.5)].

Further, invoking (36) into (34), and simplifying the required integral, the average SER of I2N FSO link can be evaluated according to following theorem.

Theorem 2: The average SER of I2N FSO link can be expressed as

$$\mathcal{P}_{SER,N}^{FSO} = \mathcal{J}_1 - \mathcal{J}_2. \quad (37)$$

where

$$\begin{aligned} \mathcal{J}_1 &= \frac{\mathcal{A}}{\pi\sqrt{\pi}} \frac{2^{\varpi+\beta-4} g^2}{\Gamma[\varpi]\Gamma[\beta]} \\ &\times \mathcal{G}_{4,7}^{6,2} \left[\left(\frac{\varpi\beta k}{\sqrt{\gamma_{I,N}^{FSO}}} \right)^2 \frac{1}{16\mathcal{B}^2} \middle| \begin{matrix} 1, \frac{1}{2}, \frac{g^2+1}{2}, \frac{g^2+2}{2} \\ \frac{g^2}{2}, \frac{g^2+1}{2}, \frac{\varpi}{2}, \frac{\varpi+1}{2}, \frac{\beta}{2}, \frac{\beta+1}{2}, 0 \end{matrix} \right], \end{aligned} \quad (38)$$

$$\begin{aligned} \mathcal{J}_2 &= \frac{\mathcal{A}}{\pi} \frac{2^{\varpi+\beta-4} g^2}{\Gamma[\varpi]\Gamma[\beta]} \\ &\times \left(\mathcal{G}_{3,7}^{6,1} \left[\left(\frac{\varpi\beta k}{\sqrt{\gamma_{I,N}^{FSO}}} \right)^2 \frac{\varphi_{th}^{FSO}}{16} \middle| \begin{matrix} 1, \frac{g^2+1}{2}, \frac{g^2+2}{2} \\ \frac{g^2}{2}, \frac{g^2+1}{2}, \frac{\varpi}{2}, \frac{\varpi+1}{2}, \frac{\beta}{2}, \frac{\beta+1}{2}, 0 \end{matrix} \right] \right. \\ &\left. - \frac{2}{\sqrt{\pi}} \sum_{t=0}^{\infty} \frac{(-1)^t \mathcal{B}^{2t+1}}{t!(2t+1)} (\varphi_{th}^{FSO})^{t+\frac{1}{2}} \times \mathcal{G}_{3,7}^{6,1} \left[\left(\frac{\varpi\beta k}{\sqrt{\gamma_{I,N}^{FSO}}} \right)^2 \frac{\varphi_{th}^{FSO}}{16} \middle| \begin{matrix} -t+\frac{1}{2}, \frac{g^2+1}{2}, \frac{g^2+2}{2} \\ \frac{g^2}{2}, \frac{g^2+1}{2}, \frac{\varpi}{2}, \frac{\varpi+1}{2}, \frac{\beta}{2}, \frac{\beta+1}{2}, -t-\frac{1}{2} \end{matrix} \right] \right). \end{aligned} \quad (39)$$

Proof: The detailed derivation is given in Appendix C. ■

ii) *Evaluation of $\mathcal{P}_{SER,N}^{RF}$* : The average SER of I2N RF link during non-outage event can be given by

$$\mathcal{P}_{SER,N}^{RF} = \int_{\varphi_{th}^{RF}}^{\infty} p(e/x) f_{\gamma_{I,N}^{RF}}(x) dx. \quad (40)$$

From (27), we can have

$$F_{\gamma_{I,N}^{RF}}(x) = \frac{1}{\Gamma[m_N]} \Upsilon \left[m_N, \frac{m_N x \sigma_N^2}{\Omega_N P_1} \right]. \quad (41)$$

By taking the derivative of (41) with the help of [32, eq. (8.350.1)], we can get the PDF of $\gamma_{I,N}^{RF}$ as

$$f_{\gamma_{I,N}^{RF}}(x) = \frac{1}{\Gamma[m_N]} \left(\frac{m_N}{\Omega_N \varrho} \right)^{m_N} x^{m_N-1} e^{-\frac{m_N x}{\Omega_N \varrho}}, \quad (42)$$

where $\varrho = \frac{P_1}{\sigma_N^2}$. Furthermore, following the similar steps as used to obtain (32), we can have

$$\begin{aligned} \mathcal{P}_{SER,N}^{RF} &= \frac{\mathcal{A}}{2} \frac{1}{\Gamma[m_N]} \operatorname{erfc} \left(\mathcal{B} \sqrt{\varphi_{th}^{RF}} \right) \Gamma \left(m_N, \frac{m_N}{\Omega_N \varrho} \varphi_{th}^{RF} \right) \\ &- \frac{\mathcal{A}\mathcal{B}}{2\sqrt{\pi}} \sum_{n=0}^{m_N-1} \frac{1}{n!} \frac{\Gamma \left(n + \frac{1}{2}, \left(\mathcal{B}^2 + \frac{m_N}{\Omega_N \varrho} \right) \varphi_{th}^{RF} \right)}{\left(\mathcal{B}^2 + \frac{m_N}{\Omega_N \varrho} \right)^{n+\frac{1}{2}}} \left(\frac{m_N}{\Omega_N \varrho} \right)^n. \end{aligned} \quad (43)$$

From the obtained expressions for $\mathcal{P}_{SER,N}^{FSO}$ and $\mathcal{P}_{SER,N}^{RF}$, one can obtain $\mathcal{P}_{SER,N}$ using (33), and consequently invoking the resultant expression along with (32) into (29), we can get the average SER, \mathcal{P}_{SER} , of the considered system.

E. Average End-to-End Delay

The average end-to-end delay is a measure of the average minimum transmission time (MTT) taken by a packet of length \mathcal{L} in transit from vehicle to network for given system bandwidth of \bar{W} and is given by

$$\mathbb{E}[\text{MTT}] = \mathbb{E}[\text{MTT}_I] + \mathbb{E}[\text{MTT}_N], \quad (44)$$

where $\mathbb{E}[\text{MTT}_I]$ and $\mathbb{E}[\text{MTT}_N]$ are the average MTTs taken by V2I and I2N hops, respectively. The expression for MTT for V2I link can be formulated as [42]

$$\text{MTT}_I = \frac{\mathcal{L}}{\bar{W} \log_2(1 + \gamma_{V,I})}, \quad (45)$$

where $\gamma_{V,I}$ is the instantaneous received SNR.

Since the I2N link involves both FSO and RF links, finding the average MTT of the I2N link requires consideration of both cases; when the FSO link is active and when the FSO link is in the outage. Therefore, end-to-end average MTT at network can be expressed as

$$\mathbb{E}[\text{MTT}_N] = (1 - \mathcal{P}_{FSO}) \mathbb{E}[\text{MTT}_N^{FSO}] + \mathcal{P}_{FSO} \mathbb{E}[\text{MTT}_N^{RF}], \quad (46)$$

where $\mathbb{E}[\text{MTT}_N^{FSO}]$ and $\mathbb{E}[\text{MTT}_N^{RF}]$ are the average MTT's taken by individual FSO and RF links of I2N link, respectively. Similar to (45), one can formulate MTT_N^{FSO} and MTT_N^{RF} using the corresponding instantaneous SNRs.

TABLE I
OPTIMAL VALUES OF α FOR MINIMIZING OUTAGE PROBABILITY

P_V (dBm)	v_s (kmph)	r_{th} (bps/Hz)	$(\mathcal{P}_{out})_{min}$	α^*
18	5	1/2	0.00009137	0.5930
21	10	1/3	0.000021847	0.6225
24	15	2/3	0.000046236	0.6665
27	20	1	0.3406	0.7135
27	20	3/2	0.7577	0.7015

TABLE II
OPTIMAL VALUES OF α FOR MAXIMIZING THROUGHPUT

P_V (dBm)	v_s (kmph)	$\bar{\gamma}_{I,N}^{FSO}$ (dB)	$(S_T)_{max}$	α^*
18	5	10	1.2126	0.4270
21	10	15	1.3395	0.4515
24	15	20	1.3501	0.5320
27	20	25	0.4924	0.7440

F. Optimization

This section proposes a time allocation factor scheme that is based on choosing α^* of α that minimizes the outage probability and maximizes the system throughput.

1) *Optimization Problem for Minimizing Outage Probability:* Here, our main objective is to minimize the outage probability of the considered system, which can be posed as

$$\begin{aligned} \alpha^* &= \arg \min_{\alpha} \mathcal{P}_{out} \\ \text{subject to: } & 0 < \alpha < 1, \end{aligned} \quad (47)$$

where \mathcal{P}_{out} is given in (21).

By obtaining the second derivative of \mathcal{P}_{out} with respect to α , one can notice that $\frac{\partial^2 \mathcal{P}_{out}}{\partial \alpha^2} > 0$, for $\alpha \in (0, 1)$. This indicates that the objective function is strictly convex function of α for the considered range. Thus, by taking the first derivative of \mathcal{P}_{out} with respect to α and equating it to zero, the optimal value of time factor α^* can be evaluated. Table I in the numerical results section elaborates the optimal values of α that minimizes the outage probability for different sets of parameters with $\bar{\gamma}_{I,N}^{FSO} = 20$ dB.

2) *Optimization Problem for Maximizing System Throughput:* Here, we optimize α by maximizing the system throughput S_T given in (28) as

$$\begin{aligned} \alpha^* &= \arg \max_{\alpha} S_T \\ \text{subject to: } & 0 < \alpha < 1. \end{aligned} \quad (48)$$

Similar to the above optimization problem, we perform the second derivative of S_T with respect to α , and observe that $\frac{\partial^2 S_T}{\partial \alpha^2} < 0$ in the interval $(0, 1)$. Accordingly, setting the first derivative of the objective function with respect to α to zero, i.e., $\frac{\partial S_T}{\partial \alpha} = 0$, we can obtain the optimal values of α . Table II in the numerical results section demonstrates the optimal values of α that maximizes the system throughput for different sets of system/channel parameters with $r_{th} = 1.5$.

IV. NUMERICAL RESULTS

In this section, we provide numerical and simulation results for the outage probability, system throughput, average SER, and

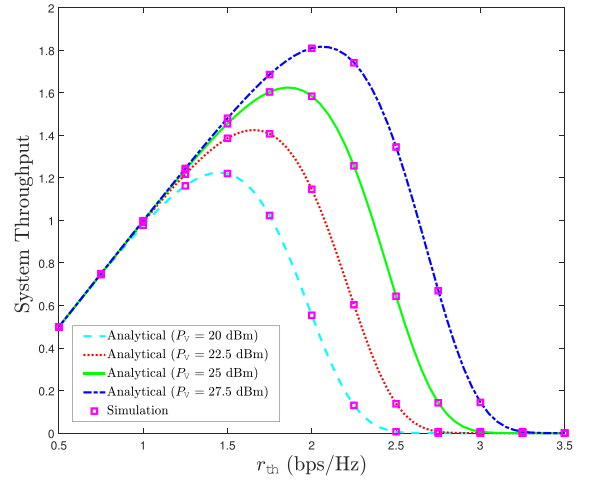


Fig. 3. System throughput versus target rate for different values of P_V .

average end-to-end delay of the considered system for different channel/system parameters. For numerical investigations, unless explicitly mentioned, we set the values as $m_I = m_N = m = 2$, $T_d = 1$ ms, $f_c = 1.9$ GHz, $c = 3 \times 10^8$ mps, $\Omega_e = 0.5$ dBm, $\sigma_I^2 = 1$ dBm, $\varpi = 5.41$, $\beta = 3.78$ [43], $w_0 = 5$ cm, $z = 1000$ m, $C_n^2 = 10^{-13}$, $\lambda = 1550$ nm, $\sigma_s = 10$ cm, $a = 14$ cm, $\Omega_I = \Omega_N = 1$, $P_I = 80$ mW, and $\sigma_N^2 = 0.008$. The typical value of transmit power of vehicles operating with cellular-V2X and IEEE 802.11p is considered as 23 dBm [44].

In Fig. 3, we show the system throughput behavior by changing the target rates with various values of vehicle transmit power P_V . Herein, we set $\bar{\gamma}_{I,N}^{FSO} = 20$ dB, $\alpha = 0.3$, and $v_s = 5$ kmph. This figure shows that the system throughput increases with the increase in target rate and reaches a maximum achievable level for a specific target rate. After that, the system throughput starts decreasing with a further increase in the target rate. This is because the threshold SNR is less for smaller values of the target rate, and thus, it attributes to better outage performance. But when the target rate becomes higher than a particular value, the outage probability starts dominating, ultimately reducing the system throughput.

The deviation of outage probability and system throughput concerning the target rate for different relative velocities are illustrated in Figs. 4 and 5, respectively. For plotting these figures, the parameters are set as $P_V = 30$ dBm, $\alpha = 0.3$, $\bar{\gamma}_{I,N}^{FSO} = 20$ dB. In order to show the importance of our proposed system, we compare its outage performance with that of the scenario where only the FSO link operates between the infrastructure and base station in Fig. 4. The improvement in the outage performance is reflected because of the backup RF link that makes communication more reliable. When the target rate is kept lower, the gap between outage probability for both cases is wider for different values of relative velocities. This gap reduces when the outage probability approaches towards unity due to increased target rates. Moreover, one can observe that the outage performance degrades when the relative velocity of the vehicle increases. This is because the correlation coefficient affects the infrastructure node's decoding probability, which

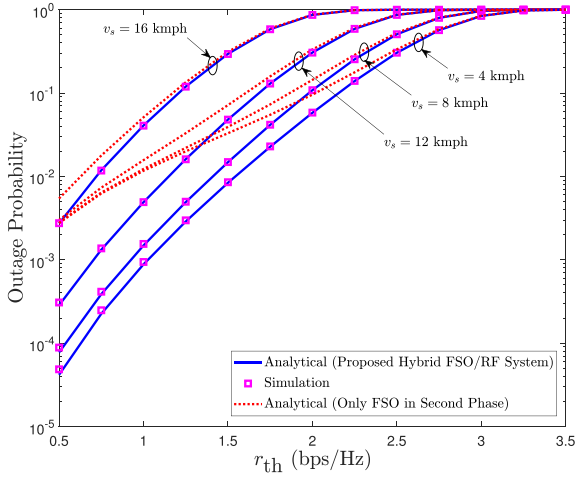


Fig. 4. Outage probability versus target rate for different values of v_s .

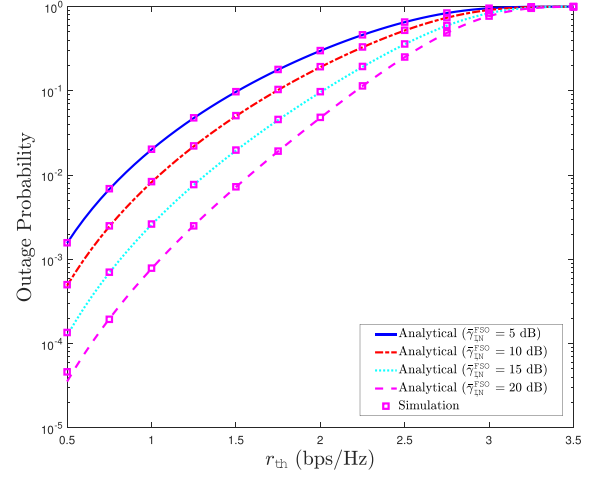


Fig. 6. Outage probability versus target rate for different values of $\bar{\gamma}_{L,N}^{FSO}$.

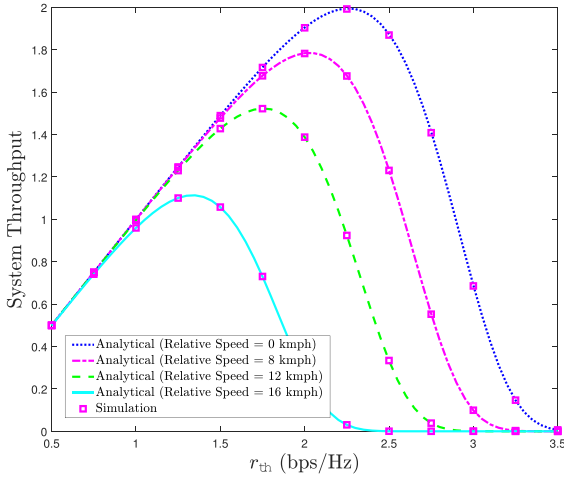


Fig. 5. System throughput versus target rate for different values of v_s .

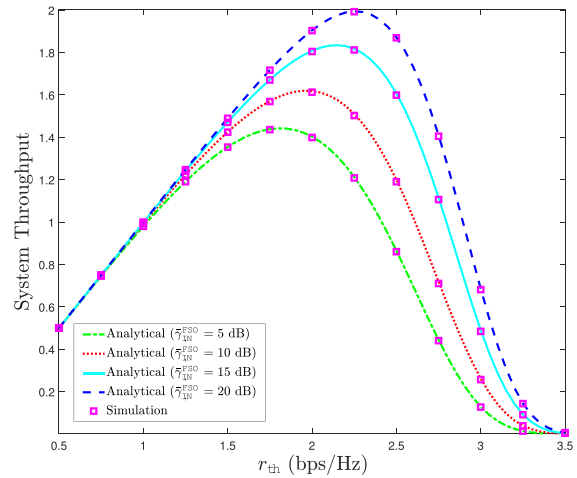


Fig. 7. System throughput versus target rate for different values of $\bar{\gamma}_{L,N}^{FSO}$.

results in a higher system outage probability. On the other hand, it is apparent from Fig. 5 that the system throughput degrades with a rise in relative velocity (as also illustrated in Fig. 4 for outage performance) due to variations in the values of the correlation coefficient. In addition, one can note that the best system performance in terms of outage probability and system throughput is accomplished when the vehicle is not moving. The system performance deteriorates significantly when the vehicle drives at a higher relative velocity.

In order to reveal the impact of the average SNR of the FSO link, we plot outage probability versus target rate curves in Fig. 6 and system throughput versus target rate curves in Fig. 7. For plotting the curves, we set $v_s = 5$ kmph, $\alpha = 0.3$, and $P_V = 30$ dBm. From Fig. 6, one can notice that the system performance in terms of outage probability improves with an increase in the average SNR of the FSO link. This behavior is manifested due to the fact that the instantaneous SNR of the FSO link rises with an increase in the average SNR of the FSO link, which results in favorable irradiance at the base station and consequently aids in the enhanced outage performance of the system. From the plots of Fig. 7, we infer that the system

throughput performance improves by increasing the average SNR of the FSO link, resulting from the gain in instantaneous SNR of the FSO link by increasing the average SNR of the FSO link.

Figs. 8 and 9 highlight the outage probability and system throughput variations with respect to α plots for various values of transmit power P_V at the vehicle. Herein, we set the parameters as $v_s = 5$ kmph and $\bar{\gamma}_{L,N}^{FSO} = 20$ dB with $r_{th} = 1$ bps/Hz in Fig. 8 and $r_{th} = 2$ bps/Hz in Fig. 9, respectively. With these figures, we highlight insights related to the optimum values of α for which the system shows desired performance in terms of system throughput and outage probability. From Fig. 8, we observe that initially, the outage performance improves as the value of α increases. Whereas, after a typical value, the outage performance starts degrading for the higher values of α . Likewise, from Fig. 9, we manifestly see improvement in system throughput with the initial increase in values of α . After a certain value, system throughput starts falling. From these two figures, one can notice that system's outage and throughput performance are better when the α spans from 0.3 to 0.4 with transmit power $P_V = 27$

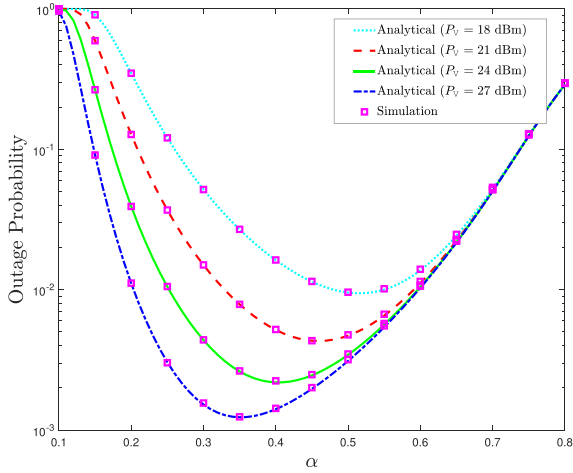


Fig. 8. Outage probability versus α for different values of P_V .

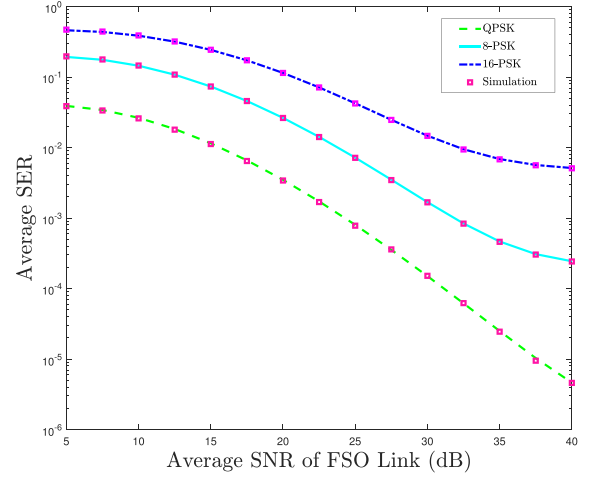


Fig. 10. \mathcal{P}_{SER} versus $\bar{\gamma}_{T,N}^{\text{FSO}}$ for different values of M .

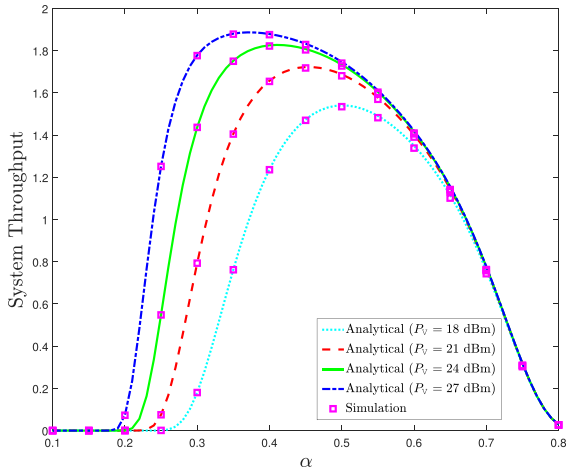


Fig. 9. System throughput versus α for different values of P_V .

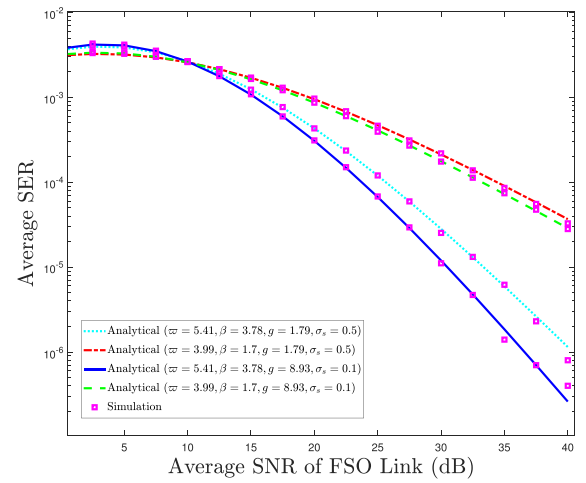


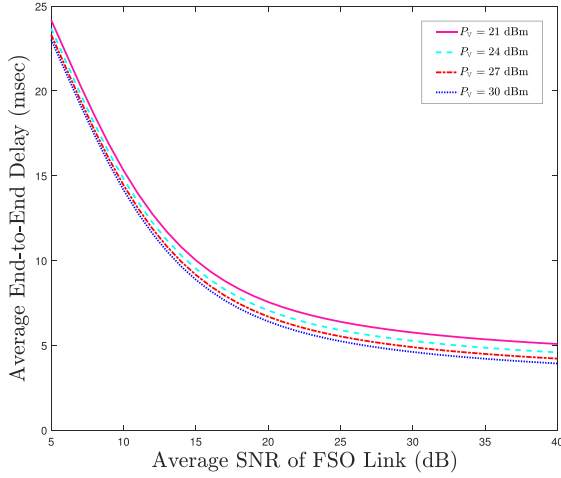
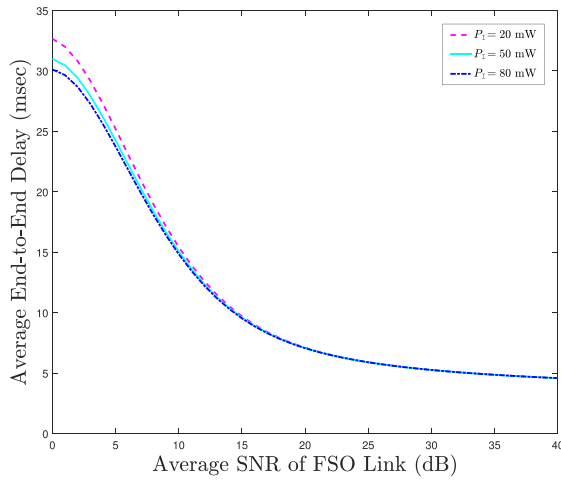
Fig. 11. \mathcal{P}_{SER} versus $\bar{\gamma}_{T,N}^{\text{FSO}}$ for different values of ϖ , β and σ_s .

dBm. Furthermore, with $P_V = 21$ and $P_V = 24$ dBm, the system exhibits desired performance for α varying from 0.4 to 0.5 and 0.35 to 0.45, respectively. As a whole, one can conclude that when P_V is set higher, the system reveals better performance with smaller values of α and when P_V is comparatively smaller, α needs to be higher.

For obtaining SER results in Figs. 10 and 11, the value of t in (39) in the expression of average SER of the FSO link is truncated to 30. Specifically, Fig. 10 plots the variation of average SER of the system against average SNR of FSO link for $M = 4, 8$, and 16. In plotting Fig. 10, the other parameters are set as $\alpha = 0.3$, $r_{\text{th}} = 1$ bps/Hz, $P_V = 27$ dBm, $v_s = 5$ kmph. From this figure, it can be seen that as the average SNR of the FSO link increases, the average SER decreases. It is due to the increase in instantaneous SNR of FSO transmission at the base station with an increase in average SNR of FSO link. Also, one can note that the SER performance deteriorates when considering a modulation scheme with lesser Euclidean distance between signaling points, i.e., by increasing modulation order M .

The impact of atmospheric turbulence-induced fading and pointing errors are highlighted in Fig. 11. The parameters are

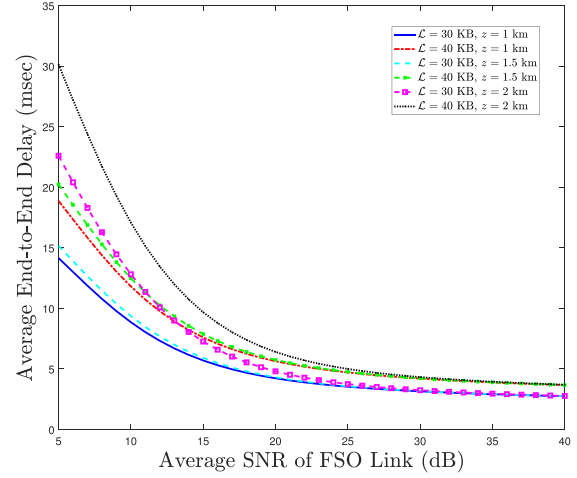
set as $\alpha = 0.3$, $r_{\text{th}} = 1$ bps/Hz, $P_V = 27$ dBm, $v_s = 5$ kmph. From this figure, one can readily observe that the severity of atmospheric turbulence from the channel varies by changing values of ϖ and β . Particularly, higher values of ϖ and β result in a smaller effect of turbulence. By considering different values of ϖ and β pair, it can be observed that the SER of the system shows better performance for $\varpi = 5.41$ and $\beta = 3.78$ than for the values of $\varpi = 3.99$ and $\beta = 1.7$. The difference in average SER performance between the two pairs increases with an increase in the average SNR of FSO link. However, for smaller values of the average SNR of the FSO link, the difference in average SER performance is negligible. This is because for smaller values of average SNR of FSO link, the possibility of FSO link in the outage is high. Thus, the backup RF link acts as the primary link, and therefore, the effect of FSO parameters becomes negligible. Similar behavior of SER can be observed for pointing errors. Due to the direct dependency of the pointing error coefficient (g) on irradiance of the FSO link and its inverse proportionality with pointing error standard deviation (σ_s), a better average SER


 Fig. 12. Average end-to-end delay versus $\bar{\gamma}_{I,N}^{\text{FSO}}$ for different values of P_V .

 Fig. 13. Average end-to-end delay versus $\bar{\gamma}_{I,N}^{\text{FSO}}$ for different values of P_I .

performance can be attained for smaller values of pointing error standard deviation.

Fig. 12 shows the variation of average end-to-end delay with average SNR of FSO link for different values of source transmit power. The parameters are set as $\mathcal{L} = 50$ KB, $\bar{W} = 20$ MHz, $\alpha = 0.3$, $r_{\text{th}} = 1$ bps/Hz, $v_s = 5$ kmph. It can be observed that with the increase in the average SNR of the FSO link, the average end-to-end delay decreases. Also, it can be noticed that with an increase in source transmit power P_V , the average end-to-end delay performance improves.

In Fig. 13, we plot the average end-to-end delay versus average SNR of FSO link curves for different values of RF transmit power of the I2N link. We set the parameters as $\mathcal{L} = 50$ KB, $\bar{W} = 20$ MHz, $\alpha = 0.3$, $r_{\text{th}} = 1$ bps/Hz, $P_V = 27$ dBm, $v_s = 5$ kmph. From this figure, one can see that for smaller values of average SNR of the FSO link, the curves with a higher value of RF transmit power shows better performance. As we increase the average SNR of the FSO link, the curves with different values of RF transmit power exhibit almost the same values of average end-to-end delay. This behavior is because of the fact that with


 Fig. 14. Average end-to-end delay versus $\bar{\gamma}_{I,N}^{\text{FSO}}$ for different values of \mathcal{L} and z .

smaller values of average SNR of FSO link, there is a high chance of FSO I2N link undergoing an outage, leading to a switch over to I2N RF link for data transmission. Thus, with the RF link being active, higher values of RF transmit power improves the average delay performance. However, with an increase in average SNR of the FSO link, the I2N link switches back to the FSO link, and there will be no influence of RF transmit power on delay performance.

We disclose the dependency of average end-to-end delay performance on FSO I2N link distance (z) and packet length \mathcal{L} in Fig. 14 for different values of average SNR of FSO link. The parameters are set to be $\mathcal{L} = 50$ KB, $\bar{W} = 20$ MHz, $\alpha = 0.3$, $r_{\text{th}} = 1$ bps/Hz, $P_V = 27$ dBm, $v_s = 5$ kmph. This figure shows that with an increase in FSO link distance, the average delay increases, and a better average delay performance can be obtained with smaller packet lengths. It can be attributed to the dependency of irradiance of the FSO link on transmission distance and the direct dependence of packet length on MTT. We can infer from the figure that average delay performance curve for $L = 30$ KB, $z = 2$ km shows better performance than $L = 40$ KB, $z = 2$ km and slightly lower in performance as compared to $L = 40$ KB, $z = 1.5$ km. This observation reveals the deterioration in delay performance due to an increase in FSO link distance can be compensated by using packets of relatively smaller length. In the results of average end-to-end delay, the inherent delay present in the system due to the conversion of RF signal to FSO signal at infrastructure is assumed to be comparatively smaller and hence ignored without loss of generality.

V. CONCLUSION

In this paper, we have proposed a system to facilitate communication from vehicles to the network with the help of transceiver-mounted roadside infrastructure. Herein, we have considered FSO transmission from infrastructure to the base station to support massive data rates with spatial confinement. An RF link operates as a backup for the FSO transmission to make the communication reliable. As the performance of the FSO link

may suffer in realistic scenarios, we have taken into account practical phenomena such as pointing errors, gamma-gamma distributed atmospheric turbulence-induced fading, and atmospheric attenuation. On the other hand, RF links are considered to follow the Nakagami- m distribution. In order to analyze the performance, we have first derived the accurate expression for the outage probability considering mixed RF and hybrid FSO/RF transmission. Moreover, we defined the system throughput utilizing the outage probability expression. Then, we obtained the accurate analytical formulation for the average symbol error rate. Additionally, we acquired an expression for the average end-to-end delay. We have provided the simulation results to verify the accuracy of all the derived analytical findings. Numerical results have revealed the impact of transmit power of the vehicle, relative velocity, pointing error coefficient, modulation scheme, packet length, and selection of time factor on outage probability, system throughput, average SER, and average end-to-end delay of the system.

APPENDIX

A. Proof of Proposition 1

We can formulate the CDF of \mathcal{I}_a as $F_{\mathcal{I}_a}(x) = \Pr[X_1 X_2 \leq x]$, and in an integral form as

$$F_{\mathcal{I}_a}(x) = \int_0^\infty \int_0^{\frac{x}{v}} f_{X_1}(v) f_{X_2}(w) dw dv. \quad (49)$$

By performing the differentiation on both sides with respect to x and considering $w = \frac{x}{v}$ and $\frac{dw}{dx} = \frac{1}{v}$, we can have the PDF of \mathcal{I}_a as

$$f_{\mathcal{I}_a}(x) = \int_0^\infty f_{X_1}(v) f_{X_2}(x/v) (1/v) dv. \quad (50)$$

By invoking the PDFs of X_1 and X_2 into (50) and simplifying the integral by utilizing [32, eq. (3.471.9)], we can obtain the desired PDF (given as (13)) as

$$f_{\mathcal{I}_a}(x) = \frac{2(\varpi\beta)^{\frac{\varpi+\beta}{2}}}{\Gamma(\varpi)\Gamma[\beta]} x^{\frac{\varpi+\beta}{2}-1} \mathcal{K}_{\varpi-\beta}(2\sqrt{\varpi\beta x}). \quad (51)$$

Furthermore, by utilizing the fact that $F_X(z) = \int_0^z f_X(x) dx$, we can obtain the CDF of \mathcal{I}_a using (51) by exploiting the transformation $\mathcal{K}_u(x) = \frac{1}{2} G_{0,2}^{2,0} \left[\frac{x^2}{4} \middle| \frac{u}{2}, \frac{-u}{2} \right]$ [45, eq. (03.04.26.0008.01)] and the relation given in [45, eq. (07.34.21.0084.01)], as presented in (14). This completes the proof.

B. Proof of Theorem 1

By using (6) and (24), we can express \mathcal{P}_{FSO} as

$$\begin{aligned} \mathcal{P}_{\text{FSO}} &= \Pr \left[\frac{\mathcal{I}_F^2}{(\mathbb{E}\{\mathcal{I}_F\})^2} \bar{\gamma}_{\text{I,N}}^{\text{FSO}} < \varphi_{\text{th}}^{\text{FSO}} \right], \\ &= F_{\mathcal{I}_F} \left(\sqrt{\frac{\varphi_{\text{th}}^{\text{FSO}} (\mathbb{E}\{\mathcal{I}_F\})^2}{\bar{\gamma}_{\text{I,N}}^{\text{FSO}}}} \right). \end{aligned} \quad (52)$$

To evaluate the expression of \mathcal{P}_{FSO} , we first need to obtain the CDF of \mathcal{I}_F and $\mathbb{E}\{\mathcal{I}_F\}$, as presented hereunder.

1) *The CDF of \mathcal{I}_F* : By utilizing the relation $\mathcal{I}_F = \mathcal{I}_a \mathcal{I}_p \mathcal{I}_l$, the PDF of \mathcal{I}_F can be represented in an integral form, considering \mathcal{I}_l to be deterministic, as

$$f_{\mathcal{I}_F}(x) = \int_0^\infty f_{\mathcal{I}_a}(v) f_{\mathcal{I}_p} \left(\frac{x}{v\mathcal{I}_l} \right) \left(\frac{1}{v\mathcal{I}_l} \right) dv. \quad (53)$$

From (17), \mathcal{I}_p can take a value from 0 to A_0 , therefore, we can have the boundary for v as $0 \leq \frac{x}{v\mathcal{I}_l} \leq A_0 \Rightarrow v \geq \frac{x}{A_0\mathcal{I}_l}$. By substituting the boundary of v along with the PDFs of \mathcal{I}_a and \mathcal{I}_p into (53), we can express the PDF of \mathcal{I}_F as

$$\begin{aligned} f_{\mathcal{I}_F}(x) &= \int_{\frac{x}{A_0\mathcal{I}_l}}^\infty \frac{2(\varpi\beta)^{\frac{\varpi+\beta}{2}}}{\Gamma[\varpi]\Gamma[\beta]} v^{\frac{\varpi+\beta}{2}-1} \mathcal{K}_{\varpi-\beta} \left(2\sqrt{\varpi\beta v} \right) \\ &\quad \times \frac{g^2}{(A_0)^{g^2}} \left(\frac{x}{v\mathcal{I}_l} \right)^{g^2-1} \left(\frac{1}{v\mathcal{I}_l} \right) dv. \end{aligned} \quad (54)$$

On utilizing the representation $\mathcal{K}_u(x) = \frac{1}{2} G_{0,2}^{2,0} \left[\frac{x^2}{4} \middle| \frac{u}{2}, \frac{-u}{2} \right]$ [45, eq. (03.04.26.0008.01)] in (54), one can get

$$\begin{aligned} f_{\mathcal{I}_F}(x) &= \frac{2g^2(\varpi\beta)^{\frac{\varpi+\beta}{2}}}{\Gamma[\varpi]\Gamma[\beta]} \frac{x^{g^2-1}}{\mathcal{I}_l^{g^2} A_0^{g^2}} \int_{\frac{x}{A_0\mathcal{I}_l}}^\infty i_a^{\frac{\varpi+\beta}{2}-g^2-1} \\ &\quad \times \frac{1}{2} \mathcal{G}_{0,2}^{2,0} \left[\varpi\beta v \middle| \frac{\varpi-\beta}{2}, \frac{-\varpi+\beta}{2} \right] dv. \end{aligned} \quad (55)$$

Then, using [45, (eq. 07.34.21.0085.01)], the PDF $f_{\mathcal{I}_F}(x)$ can be expressed as

$$\begin{aligned} f_{\mathcal{I}_F}(x) &= \frac{g^2}{\Gamma[\varpi]\Gamma[\beta]} \left(\frac{\varpi\beta}{A_0\mathcal{I}_l} \right)^{\frac{\varpi+\beta}{2}} x^{\frac{\varpi+\beta}{2}-1} \\ &\quad \times \mathcal{G}_{1,3}^{3,0} \left[\frac{\varpi\beta x}{A_0\mathcal{I}_l} \middle| g^2 - \frac{\varpi+\beta}{2} + 1, g^2 - \frac{\varpi+\beta}{2}, -\frac{\varpi+\beta}{2} \right]. \end{aligned} \quad (56)$$

Furthermore, by integrating (56) with the aid of [45, eq. (07.34.21.0084.01)], we can express the CDF of \mathcal{I}_F as

$$\begin{aligned} F_{\mathcal{I}_F}(x) &= \frac{g^2}{\Gamma[\varpi]\Gamma[\beta]} \left(\frac{\varpi\beta}{A_0\mathcal{I}_l} \right)^{\frac{\varpi+\beta}{2}} x^{\frac{\varpi+\beta}{2}} \\ &\quad \times \mathcal{G}_{2,4}^{3,1} \left[\frac{\varpi\beta x}{A_0\mathcal{I}_l} \middle| 1 - \frac{\varpi+\beta}{2}, g^2 - \frac{\varpi+\beta}{2} + 1, g^2 - \frac{\varpi+\beta}{2}, -\frac{\varpi+\beta}{2} \right], \end{aligned} \quad (57)$$

which can be then simplified by using [32, eq. (9.31.5)], to obtain the CDF of \mathcal{I}_F as

$$F_{\mathcal{I}_F}(x) = \frac{g^2}{\Gamma[\varpi]\Gamma[\beta]} \mathcal{G}_{2,4}^{3,1} \left[\frac{\varpi\beta x}{A_0\mathcal{I}_l} \middle| 1, g^2 + 1, g^2, \varpi, \beta, 0 \right]. \quad (58)$$

2) *Evaluation of $\mathbb{E}\{\mathcal{I}_F\}$* : We can express the average value of \mathcal{I}_F as $\mathbb{E}\{\mathcal{I}_F\} = \mathbb{E}\{\mathcal{I}_a\} \mathbb{E}\{\mathcal{I}_p\} \mathbb{E}\{\mathcal{I}_l\}$. On assuming $\mathbb{E}\{\mathcal{I}_a\}$ to be unity with $\mathbb{E}\{\mathcal{I}_l\}$ being deterministic signal, we can have $\mathbb{E}\{\mathcal{I}_F\} = \mathbb{E}\{\mathcal{I}_p\} \mathcal{I}_l$. Further, $\mathbb{E}\{\mathcal{I}_p\}$ can be evaluated using (17) as

$$\begin{aligned} \mathbb{E}\{\mathcal{I}_p\} &= \int_0^{A_0} x \frac{g^2}{(A_0)^{g^2}} x^{g^2-1} dx \\ &= A_0 \frac{g^2}{g^2 + 1}. \end{aligned} \quad (59)$$

Now, we can represent the average value of \mathcal{I}_F as

$$\mathbb{E}\{\mathcal{I}_F\} = A_0\mu\mathcal{I}_l, \quad (60)$$

where $\mu = \frac{g^2}{g^2+1}$. Consequently, the average electrical SNR of the FSO link at the base station, $\bar{\gamma}_{I,N}^{\text{FSO}} = \frac{P_{\text{IF}}^2\eta^2(\mathbb{E}\{\mathcal{I}_F\})^2}{\sigma_{\text{NF}}^2}$, can be expressed as $\bar{\gamma}_{I,N}^{\text{FSO}} = \frac{P_{\text{IF}}^2\eta^2(A_0\mu\mathcal{I}_l)^2}{\sigma_{\text{NF}}^2}$.

Now, substituting (58) and (60) into (52), and after some simplifications, we can obtain the probability of failure of FSO link, \mathcal{P}_{FSO} , as presented in (25).

C. Proof of Theorem 2

We first express the average SER given in (34) as

$$\mathcal{P}_{\text{SER},N}^{\text{FSO}} = \underbrace{\int_0^{\varphi_{\text{th}}^{\text{FSO}}} p(e/x) f_{\gamma_{I,N}^{\text{FSO}}}(x) dx}_{\triangleq \mathcal{J}_1} - \underbrace{\int_0^{\varphi_{\text{th}}^{\text{FSO}}} p(e/x) f_{\gamma_{I,N}^{\text{FSO}}}(x) dx}_{\triangleq \mathcal{J}_2}. \quad (61)$$

Now, invoking the PDF $f_{\gamma_{I,N}^{\text{FSO}}}(x)$ from (36) along with the simplified relation of $p(e/x) = \frac{A}{2} \text{erfc}(\mathcal{B}\sqrt{x}) = \frac{A}{2\sqrt{\pi}} G_{1,2}^{2,0} \left[\mathcal{B}^2 x \middle|_{0, \frac{1}{2}}^1 \right]$ (which can be obtained by applying the transformation [45, (eq. 07.34.03.0619.01)]) into \mathcal{J}_1 of (61), we can obtain

$$\mathcal{J}_1 = \frac{A}{2\sqrt{\pi}} \frac{g^2}{2\Gamma[\varpi]\Gamma[\beta]} \int_0^{\varphi_{\text{th}}^{\text{FSO}}} \frac{1}{x} G_{1,2}^{2,0} \left[\mathcal{B}^2 x \middle|_{0, \frac{1}{2}}^1 \right] \times G_{1,3}^{3,0} \left[\varpi\beta k \sqrt{\frac{x}{\bar{\gamma}_{I,N}^{\text{FSO}}}} \middle|_{g^2, \varpi, \beta}^{g^2+1} \right] dx, \quad (62)$$

which can be simplified by using [45, (eq. 07.34.21.0013.01)] to obtain \mathcal{J}_1 , as presented in (38).

Furthermore, substituting the PDF $f_{\gamma_{I,N}^{\text{FSO}}}(x)$ from (36) along with the simplified transformation of $p(e/x) = \frac{A}{2} \text{erfc}(\mathcal{B}\sqrt{x}) = \frac{A}{2} \left(1 - \frac{2}{\sqrt{\pi}} \sum_{t=0}^{\infty} \frac{(-1)^t (\mathcal{B}\sqrt{x})^{2t+1}}{t!(2t+1)} \right)$ (which can be obtained by using the relation [32, eq. (3.321.1)]) into \mathcal{J}_2 of (61), we can get

$$\mathcal{J}_2 = \frac{A}{2} \left[\int_0^{\varphi_{\text{th}}^{\text{FSO}}} \frac{g^2}{2\Gamma[\varpi]\Gamma[\beta]} \frac{1}{x} G_{1,3}^{3,0} \left[\varpi\beta k \sqrt{\frac{x}{\bar{\gamma}_{I,N}^{\text{FSO}}}} \middle|_{g^2, \varpi, \beta}^{g^2+1} \right] dx - \frac{2}{\sqrt{\pi}} \sum_{t=0}^{\infty} \frac{(-1)^t (\mathcal{B})^{2t+1}}{t!(2t+1)} \frac{g^2}{2\Gamma[\varpi]\Gamma[\beta]} \times \int_0^{\varphi_{\text{th}}^{\text{FSO}}} x^{t-\frac{1}{2}} G_{1,3}^{3,0} \left[\varpi\beta k \sqrt{\frac{x}{\bar{\gamma}_{I,N}^{\text{FSO}}}} \middle|_{g^2, \varpi, \beta}^{g^2+1} \right] dx \right]. \quad (63)$$

Now, by simplifying the required integrals in (63) with the help of [45, (eq. 07.34.21.0084.01)], we can obtain \mathcal{J}_2 as given in (39). This completes the proof.

REFERENCES

- [1] H. Peng, L. Liang, X. Shen, and G. Y. Li, "Vehicular communications: A network layer perspective," *IEEE Trans. Veh. Technol.*, vol. 68, no. 2, pp. 1064–1078, Feb. 2019.
- [2] L. Miao, S.-F. Chen, Y.-L. Hsu, and K.-L. Hua, "How does C-V2X help autonomous driving to avoid accidents?," *Sensors*, vol. 22, no. 2, 2022, Art. no. 686.
- [3] B. Ji et al., "Survey on the internet of vehicles: Network architectures and applications," *IEEE Commun. Standards Mag.*, vol. 4, no. 1, pp. 34–41, Mar. 2020.
- [4] H. Zhou, W. Xu, J. Chen, and W. Wang, "Evolutionary V2X technologies toward the internet of vehicles: Challenges and opportunities," *Proc. IEEE*, vol. 108, no. 2, pp. 308–323, Feb. 2020.
- [5] "DSRC Standards: What's New?" ITS Standards Advisory number 3, US Department of Transportation, Washington, DC, USA, Apr. 2003.
- [6] FCC modernizes 5.9 GHz band to improve Wi-Fi and automotive safety Federal Communications Commission, Washington, DC, USA, Nov. 2020.
- [7] S. Fatahi-Bafqi, Z. Zeinalpour-Yazdi, and A. Asadi, "Analytical framework for mmWave-enabled V2X caching," *IEEE Trans. Veh. Technol.*, vol. 70, no. 1, pp. 585–599, Jan. 2021.
- [8] A. Alalawi, I. Dayoub, and S. Cherkaoui, "On 5G-V2X use cases and enabling technologies: A comprehensive survey," *IEEE Access*, vol. 9, pp. 107710–107737, 2021.
- [9] S. Huang, M. Zhang, Y. Gao, and Z. Feng, "MIMO radar aided mmWave time-varying channel estimation in MU-MIMO V2X communications," *IEEE Trans. Wireless Commun.*, vol. 20, no. 11, pp. 7581–7594, Nov. 2021.
- [10] M. He, J. Ni, Y. He, and N. Zhang, "Low-complexity phased-array physical layer security in millimeter-wave communication for cybertwin-driven V2X applications," *IEEE Trans. Veh. Technol.*, vol. 71, no. 5, pp. 4573–4583, May 2022.
- [11] L. Zhao et al., "Vehicular communications: Standardization and open issues," *IEEE Commun. Standards Mag.*, vol. 2, no. 4, pp. 74–80, Dec. 2018.
- [12] A. Kose, H. Lee, C. H. Foh, and M. Dianati, "Beam-based mobility management in 5G millimetre wave V2X communications: A survey and outlook," *IEEE Open J. Intell. Transp. Syst.*, vol. 2, pp. 347–363, Apr. 2021.
- [13] M. Z. Chowdhury, M. Shahjalal, M. K. Hasan, and Y. M. Jang, "The role of optical wireless communication technologies in 5-G/6-G and IoT solutions: Prospects, directions, and challenges," *Appl. Sci.*, vol. 9, no. 20, 2019, Art. no. 4367.
- [14] H. Haas, J. Elmirghani, and I. White, "Optical wireless communication," *Philos. Trans. Roy. Soc. A*, vol. 378, no. 2169, pp. 1–11, 2020.
- [15] M. A. Khalighi and M. Uysal, "Survey on free space optical communication: A communication theory perspective," *IEEE Commun. Surv. Tut.*, vol. 16, no. 4, pp. 2231–2258, Oct.–Dec. 2014.
- [16] I. K. Son and S. Mao, "A survey of free space optical networks," *Digit. Commun. Netw.*, vol. 3, no. 2, pp. 67–77, 2017.
- [17] E. Balti and M. Guizani, "Mixed RF/FSO cooperative relaying systems with co-channel interference," *IEEE Trans. Commun.*, vol. 66, no. 9, pp. 4014–4027, Sep. 2018.
- [18] O. M. S. Al-Ebraheemy, A. M. Salhab, A. Chaaban, S. A. Zummo, and M.-S. Alouini, "Precise performance analysis of dual-hop mixed RF/unified-FSO DF relaying with heterodyne detection and two IM-DD channel models," *IEEE Photon. J.*, vol. 11, no. 1, pp. 1–22, Feb. 2019.
- [19] X. Yi, C. Shen, P. Yue, Y. Wang, and Q. Ao, "Performance of decode-and-forward mixed RF/FSO system over $\kappa - \mu$ shadowed and exponentiated weibull fading," *Opt. Commun.*, vol. 439, pp. 103–111, May 2019.
- [20] H. Liang, C. Gao, Y. Li, M. Miao, and X. Li, "Analysis of selection combining scheme for hybrid FSO/RF transmission considering misalignment," *Opt. Commun.*, vol. 435, pp. 399–404, 2019.
- [21] N. Vishwakarma and R. Swaminathan, "Performance analysis of hybrid FSO/RF communication over generalized fading models," *Opt. Commun.*, vol. 487, 2021, Art. no. 126796.
- [22] M. A. Amirabadi and V. T. Vakili, "Performance of a relay-assisted hybrid FSO/RF communication system," *Phys. Commun.*, vol. 35, 2019, Art. no. 100729.
- [23] A. K. Meshram, D. S. Gurjar, and P. K. Upadhyay, "Joint impact of nodes-mobility and channel estimation error on the performance of two-way relay systems," *Phys. Commun.*, vol. 23, pp. 103–113, 2017.
- [24] N. Varshney and P. Puri, "Performance analysis of decode-and-forward-based mixed MIMO-RF/FSO cooperative systems with source mobility and imperfect CSI," *J. Lightw. Technol.*, vol. 35, no. 11, pp. 2070–2077, Jun. 2017.
- [25] N. Varshney, A. K. Jagannatham, and P. K. Varshney, "Cognitive MIMO-RF/FSO cooperative relay communication with mobile nodes and imperfect channel state information," *IEEE Trans. Cogn. Commun. Netw.*, vol. 4, no. 3, pp. 544–555, Sep. 2018.
- [26] A. Pandey and S. Yadav, "Joint impact of nodes mobility and imperfect channel estimates on the secrecy performance of cognitive radio vehicular networks over Nakagami-m fading channels," *IEEE Open J. Veh. Technol.*, vol. 2, pp. 289–309, 2021, doi: 10.1109/OJVT.2021.3087637.

- [27] J. Wang, J. Liu, and N. Kato, "Networking and communications in autonomous driving: A survey," *IEEE Commun. Surv. Tut.*, vol. 21, no. 2, pp. 1243–1274, Apr.–Jun. 2019.
- [28] M. H. C. Garcia et al., "A tutorial on 5G NR V2X communications," *IEEE Commun. Surv. Tut.*, vol. 23, no. 3, pp. 1972–2026, Jul.–Sep. 2021.
- [29] M. Harounabadi, D. M. Soleymani, S. Bhadauria, M. Leyh, and E. Roth-Mandutz, "V2X in 3GPP standardization: NR sidelink in release-16 and beyond," *IEEE Commun. Standards Mag.*, vol. 5, no. 1, pp. 12–21, Mar. 2021.
- [30] F. Arena, G. Pau, and A. Severino, "A review on IEEE 802.11 p for intelligent transportation systems," *J. Sensor Actuator Netw.*, vol. 9, no. 2, 2020, Art. no. 22.
- [31] G. Naik, B. Choudhury, and J.-M. Park, "IEEE 802.11 bd & 5-G NR V2X: Evolution of radio access technologies for V2X communications," *IEEE Access*, vol. 7, pp. 70169–70184, 2019.
- [32] I. S. Gradshteyn and I. M. Ryzhik, *Table of Integrals, Series, and Products*. Cambridge, MA, USA: Academic press, 2014.
- [33] V. S. V. Sandeep, D. S. Gurjar, Y. Jiang, S. Yadav, and P. Pattanayak, "Performance of V2N communication system with mixed RF and hybrid FSO/RF transmissions," in *Proc. IEEE 95th Veh. Technol. Conf.*, 2022, pp. 1–6.
- [34] A. Al-Habash, L. C. Andrews, and R. L. Phillips, "Mathematical model for the irradiance probability density function of a laser beam propagating through turbulent media," *Opt. Eng.*, vol. 40, no. 8, pp. 1554–1562, 2001.
- [35] A. A. Farid and S. Hranilovic, "Outage capacity optimization for free-space optical links with pointing errors," *J. Lightw. Technol.*, vol. 25, no. 7, pp. 1702–1710, Jul. 2007.
- [36] Y. Khattabi and M. M. Matalgah, "Performance analysis of AF cooperative networks with time-varying links: Outage probability," in *Proc. Wireless Telecommun. Symp.*, 2014, pp. 1–6.
- [37] Y. M. Khattabi and M. M. Matalgah, "Performance analysis of multiple-relay AF cooperative systems over rayleigh time-selective fading channels with imperfect channel estimation," *IEEE Trans. Veh. Technol.*, vol. 65, no. 1, pp. 427–434, Jan. 2016.
- [38] S. Sharma, A. Madhukumar, and R. Swaminathan, "Effect of pointing errors on the performance of hybrid FSO/RF networks," *IEEE Access*, vol. 7, pp. 131418–131434, 2019.
- [39] S. S. Muhammad, B. Flecker, E. Leitgeb, and M. Gebhart, "Characterization of fog attenuation in terrestrial free space optical links," *Opt. Eng.*, vol. 46, no. 6, 2007, Art. no. 0 66001.
- [40] Y. Liu, L. Wang, M. ElKashlan, T. Q. Duong, and A. Nallanathan, "Two-way relay networks with wireless power transfer: Design and performance analysis," *IET Commun.*, vol. 10, no. 14, pp. 1810–1819, 2016.
- [41] M. J. Hossain, P. K. Vitthaladevuni, M.-S. Alouini, V. K. Bhargava, and A. J. Goldsmith, "Adaptive hierarchical modulation for simultaneous voice and multiclass data transmission over fading channels," *IEEE Trans. Veh. Technol.*, vol. 55, no. 4, pp. 1181–1194, Jul. 2006.
- [42] H.-C. Yang and M.-S. Alouini, "Wireless transmission of Big Data: Data-oriented performance limits and their applications," 2018, *arXiv:1805.09923*.
- [43] S. Anees and M. R. Bhatnagar, "Performance of an amplify-and-forward dual-hop asymmetric RF–FSO communication system," *J. Opt. Commun. Netw.*, vol. 7, no. 2, pp. 124–135, 2015.
- [44] V. Mannoni, V. Berg, S. Sesia, and E. Perraud, "A comparison of the V2X communication systems: ITS-G5 and C-V2X," in *Proc. IEEE 89th Veh. Technol. Conf.*, 2019, pp. 1–5.
- [45] The wolfram functions site, Accessed: Oct. 5, 2022. [Online]. Available: <http://functions.wolfram.com/>